The nanosizing of fluorescent objects by 458 nm spatially modulated illumination microscopy using a simplified size evaluation algorithm

2004 J. Phys.: Condens. Matter 16 S2393

(http://iopscience.iop.org/0953-8984/16/26/012)

INSTITUTE OF PHYSICS PUBLISHING JOURNAL OF PHYSICS: CONDENSED MATTER

J. Phys.: Condens. Matter **16** (2004) S2393–S2404 PII: S0953-8984(04)77589-X

The nanosizing of fluorescent objects by 458 nm spatially modulated illumination microscopy using a simplified size evaluation algorithm

Andreas Schweitzer, Christian Wagner and Christoph Cremer

Kirchhoff-Institute for Physics of the University, Im Neuenheimer Feld 227, 69120 Heidelberg, Germany

E-mail: cremer@kip.uni-heidelberg.de

Received 5 March 2004
Published 18 June 2004
Online at stacks.iop.org/JPhysCM/16/S2393
doi:10.1088/0953-8984/16/26/012

Abstract

In fluorescent light microscopy, structured illumination approaches have emerged as a novel tool to analyse subwavelength sized objects in thick transparent specimens. In this report, new size measurements ('nanosizing') of small subwavelength sized fluorescent objects applying spatially modulated illumination (SMI) microscopy with an excitation wavelength of $\lambda_{ex} = 458$ nm are presented. These measurements were made using fluorescent particles with a given diameter. From the SMI data achieved, the size (diameter) was determined using special calibration curves derived from analytical considerations assuming a Gaussian dye distribution within the object. The results showed that with SMI microscopy combined with suitable calibration, size measurements of objects considerably smaller than the epifluorescent optical resolution at $\lambda_{ex} = 458$ nm are feasible.

1. Introduction

The structural analysis of small objects is of utmost importance in many areas of science and thus one of the main applications of microscopy. In molecular cell biology, for example, an important goal is to obtain spatial information about three-dimensional nanostructures of large macromolecule complexes (BioMolecular Machines, BMM). Such biomolecular machines usually have a size in the range of some 100 nm or less. Also, the analysis of individual specific chromatin regions is important for a better understanding of the functional topology of the genome [1–3]. In recent years, substantial progress in the structure analysis of biomolecular machines was achieved using electron-, atomic-force and scanning-nearfield microscopy. For a variety of reasons, it should be highly desirable to complement such methods by light optical

'nanoscopy' approaches. Such methods would allow low photon energy analysis of fluorescent nanostructures in intact cells, eventually even '*in vivo*'.

For the analysis of biological nanostructures beyond the conventional optical resolution limits of about half the wavelength used, novel far-field microscopic methods have been developed, such as point spread function (PSF) engineering with focusing light, e.g. 4Pi [4–6] and stimulated emission depletion microscopy [7–9], or structured illumination approaches, like standing wave and spatially modulated illumination (SMI) microscopy [10–14]. Most recently, other structured illumination schemes using patterned illumination have been developed for improved nanostructural analysis [15, 16]. While from the theoretical point of view, an increase in the optical resolution of the microscope system in the sense of an appropriate modification of the PSF or the optical transfer function (OTF), respectively, may be regarded as the optimum solution [17], in many cases of practical importance it may be sufficient to improve the resolution of specific structural features. In the analysis of BMMs, for example, such structural features may be the overall size (diameter) of a BMM ('nanosizing'); or the relative position of subunits and their mutual distances within [18].

Theoretical considerations [19] and experimental results [20] have shown that nanosizing of fluorescent objects down to a small fraction of the exciting wavelength using SMI microscopy is feasible by one-photon excitation of 'optically isolated' fluorescent objects labelled with one spectral signature. Here, optical isolation means that the minimum distance between neighbouring objects has to be equal to or larger than the optical resolution. In many biologically important problems, this condition can be realized. Furthermore, conventional object preparations can be used. Using excitation wavelengths of $\lambda_{ex} = 488$ and 647 nm, the diameter of fluorescent objects was determined down to a range of a few tens of nanometres.

For a full range of applications of the SMI-nanosizing method, it will be of great importance to extend the spectrum of usable excitation wavelengths. For example, in cell biology fluorochrome labelling is often realized by genetic engineering and thus can be changed only at impractically high labour and time costs. Consequently, in such cases it is required to adapt the excitation wavelength to the fluorochrome used. Another major reason to extend the excitation spectrum is the prospect of using multicolour SMI microscopy for a highly improved topological and colocalization analysis by spectral precision distance microscopy (SPDM) [18, 21]. In the present report, for the first time size measurements of fluorescent objects using SMI microscopy with an excitation wavelength of $\lambda_{ex} = 458$ nm are presented, thus extending SMI-nanosizing to three wavelengths. The wavelength used here is adequate to excite cyan fluorescent protein (CFP) and other fluorophores commonly used in biological research.

In previous studies using $\lambda_{ex} = 488$ and 647 nm excitation, nanosizing was based on calibration curves derived from computer simulations (Virtual Microscopy, VIM) of the emission/detection process [19]. In this publication, a simplified method to derive the calibration curves was used.

2. Materials and methods

2.1. Specimens

To study the optical properties of the SMI microscope, to measure axial intensity distributions and to perform SMI-nanosizing, fluorescent microspheres (beads) were used as objects. In this case we used green fluorescent nanoparticles ($\lambda_{ex} = 468$ nm, $\lambda_{em} = 508$ nm) with different diameters of $d = 57$, 71, 100, 140 and 200 nm (Duke Scientific Corporation, Palo Alto, CA, USA). The 'actual' diameters mentioned were provided by the manufacturer. For sample preparation, 10 μl of a solution of beads diluted by a factor 200 were deposited on a conventional

object slide (76 mm × 26 mm × 1 mm) and embedded by use of the embedding medium Vectashield (Vector Laboratories, Burlingame, CA, USA). This preparation was covered by a conventional cover slip (thickness 170 μm).

2.2. The SMI microscope set-up

The general set-up of an SMI microscope has previously been described [11, 13]. The main part of this microscope is the interferometer stretched by a 50:50 beam splitter. Thus two coherent counterpropagating collimated laser beams with a diameter of approximately 10 mm were focussed into the back focal plane of two opposite objective lenses (oil immersion, MIC 700, 100-fold, NA = 1.25; Euromex microscopen BV, Arnhem, The Netherlands) by use of two achromatic focusing lenses (f = 80 mm, PAC 364, Newport, Darmstadt, Germany). This leads to a standing wave field in the interspace between the two objective lenses by interference which is characterized by a $\cos^2$-shape of the intensity along the optical axis defined by the common axis of the two objective lenses. Whereas in the former SMI microscope, excitation wavelengths of λ_{ex} = 488 and 647 nm were used, here for the excitation a multi-line Ar^+-laser with an output power of P = 2 W was applied to achieve a power of approximately P = 20 mW on the λ_{ex} = 458 nm line (Innova 310, Coherent, Inc., Santa Clara, CA, USA).

The objects deposited on object slides were placed in the space between the two opposing objective lenses. When the measurements were made, the objects were moved along the axial direction providing optical sectioning by use of a piezoelectric stage (Physik Instrumente, Waldbronn, Germany) with a step size of 20 nm. The positional resolution of the object stage was around 1 nm. The piezoelectric object stage itself was attached to a step motor-powered object stage for the macroscopic movement of the object slide, i.e., providing lateral translation for the searching of suitable objects and moving the object slide in or out of the interspace between the objectives.

The fluorescence light was detected by a CCD camera (Imager 3, LaVision GmbH, Göttingen, Germany) after it had been separated from the excitation light by a special dichroic beam splitter ($R > 90\%@\lambda \geqslant 500$ nm, $T > 80\%@\lambda \leqslant 488$ nm, Laseroptik GmbH, Garbsen, Germany). The CCD camera provides a quantum efficiency of 40–50% in the visible range. The whole microscope was mounted on a horizontal optical breadboard made of SuperInvar, which is a special material with very little thermal expansion. Thus the object slide had a vertical orientation. All electronic components, i.e. the CCD camera, step motors and piezo stages, were controlled by self-developed software on a personal computer running under Windows 2000.

We obtained a sequence of 300–400 two-dimensional images of the object plane acquired at equidistant (precision ±1 nm) axial positions. This resulted in a maximum scan volume of 6.9 μm × 8.6 μm × 8 μm = 475 μm^3. Using an integration time of about 0.4 s, a whole sequence of 400 images (representing the 3D image) takes about 400 × 0.4 s = 160 s. The experimental set-up is shown in figure 1.

2.3. The confocal laser scanning microscope

For comparative measurements we applied a conventional confocal laser scanning microscope (TCS NT, Leica Microsystems GmbH, Mannheim, Germany). This microscope was equipped with an argon krypton ion laser which provided an excitation wavelength of λ_{ex} = 488 nm, and an objective lens with oil immersion 63-fold magnification and NA = 1.4. To perform the confocal measurements, a two-dimensional scan with 16 accumulations in each axial section was done, and the fluorescence intensity in the 'green channel' was detected by

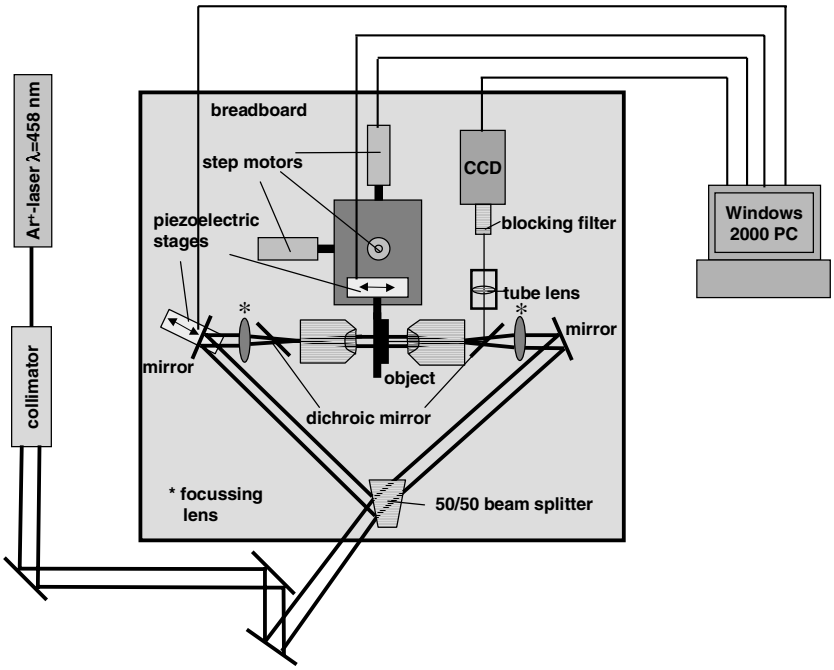

Figure 1. A schematic representation of the SMI microscope set-up using an excitation wavelength of $\lambda_{ex} = 458$ nm.

a photomultiplier. For a complete acquisition of the whole object in the axial direction approximately 20–24 axial sections providing a step width of 162 nm were required.

2.4. The principles of size evaluation

The object size S (the extension of the object in the direction of the optical axis) can be obtained by determining the modulation contrast R of the measured axial intensity distribution of the object (for a general description see [19, 20]). Figure 2 illustrates this in principle, using simulated curves. Under the assumption of a Gaussian fluorochrome distribution inside the objects, there is a strictly monotonically increasing relationship between object size and modulation contrast, i.e. the smaller the object the lower the measured R-value. Figure 3 depicts a calibration curve showing this relation for the assumptions we made (see above). To determine the relationship between R and S, one can use different approaches. Up to now we used virtual microscopy (VIM), i.e. 3D computer simulations of the excitation/detection process of the SMI microscope. For the measurements presented here, we applied a simplified mathematical model in which we assumed (as was done in the VIM-simulations) that the dye distribution within one object follows a Gaussian-distribution, where the FWHM is equivalent to the diameter of the object [24]. Taking into account that the different parts of the object sphere are excited by different light fields, the total emission intensity may be given as

$$I_{\mathrm{em}}(z) = k \int_{-\infty}^{\infty} \cos^2\left(\frac{2n\pi}{\lambda_{\mathrm{eff}}}(a-z)\right) \mathrm{e}^{-4\ln(2)a^2/d^2}\,\mathrm{d}a, \tag{1}$$

where a is the integration variable, d is the diameter of the object, k a scaling factor, z the axial position of the object, and λ_{eff} the effective wavelength. The measured distances between the maxima of the excitation light field intensity may differ from the values assuming parallel

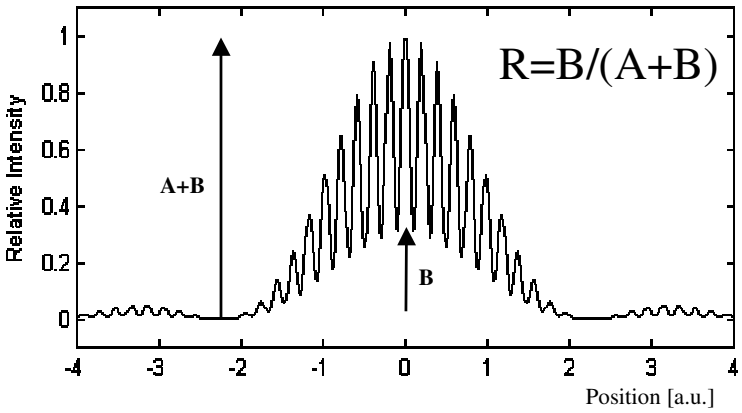

Figure 2. The schematic axial intensity distribution (AID $= I_{\mathrm{det}}(z)$) of a non-pointlike object of diameter d produced by the SMI microscope. A denotes the maximum amplitude of the modulated part of the function whereas B is the maximum amplitude of the unmodulated 'internal background'. The modulation contrast R is defined to be $B/(A + B)$.

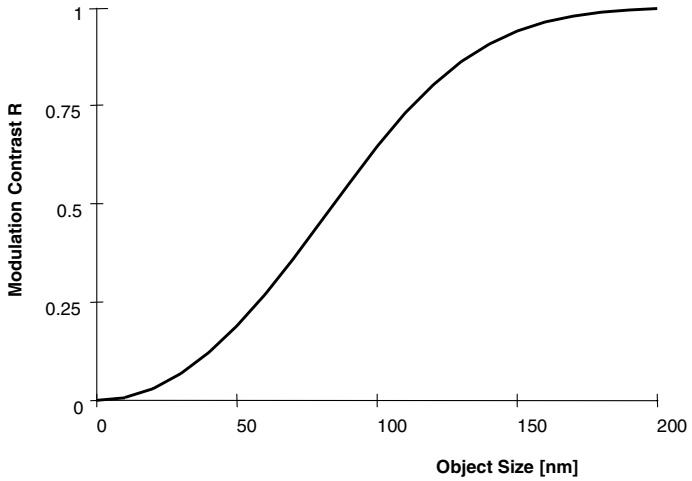

Figure 3. The calibration curve for an excitation wavelength of $\lambda_{\mathrm{ex}} = 458$ nm assuming a Gaussian dye distribution within the spherical objects. Size = FWHM of the Gaussian distribution (diameter). The calculations do not include variations induced by photon count statistics [19] and other sources of noise.

counterpropagating beams. These distances increase with larger angles between the beams. The theoretical excitation wavelength necessary to explain these distances assuming parallel counterpropagating beams is called the effective wavelength. We can calculate the modulation contrast R approximately by determining the minimum and maximum of the function I and dividing them: $R = I_{\mathrm{min}}/I_{\mathrm{max}}$. In this simplified model we did not consider that the different parts of the sphere are also differently detected, i.e. we did not consider the point spread function of the detection system. Only the emitted light intensity at different positions of the sphere in the wavefield were compared. We found no significant differences from the curves obtained by VIM assuming high fluorescence photon counts.

Table 1. A summary of the measured object sizes. The error is given by the standard deviation of the single measurement.

Actual size (nm)	Measured size (nm)	Number of evaluated objects
57	78 ± 8	11
71	93 ± 5	8
100	103 ± 12	13
140	126 ± 9	14
200	150 ± 14	7

2.5. Data evaluation

The experiments described here were made using green fluorescent beads ($\lambda_{ex} = 468$ nm, $\lambda_{em} = 508$ nm) of different sizes. Therefore object slides with these beads were placed between the two objectives of the SMI microscope. The density of beads was adjusted by diluting the solution of beads in such a way that individual small diffraction limited objects can be observed.

For the determination of the object size, one sequence of images for each actual object size was measured at $\lambda_{ex} = 458$ nm excitation. In each data stack 10–15 objects were randomly selected and evaluated. In these cases, the signal-to-noise ratio was between 5 and 10. The axial intensity distributions (AIDs) for the selected objects were extracted by setting a region of interest of 3×3 pixels around the object followed by subtraction of the background noise using a segmentation value of 20% of the maximum intensity for each of the 400 images of a 3D data stack. During this part of the evaluation, some objects were abandoned as it was not possible to determine a fit function. This was especially the case with small objects because their signal-to-noise ratio was low. Some asymmetric AIDs or distributions with very high peaks coming from the short time detection of moving objects in the mounting or immersion medium were also not taken into account. Figure 4 illustrates some measured axial intensity distributions of beads with different sizes. As the objects are not pointlike, the intensities in the local minima of the axial intensity distribution are larger than zero. Therefore, the measured data have to be described by a special fit function, which differs from the SMI point spread function by taking the depth of modulation into account. Here, we determined a fit function of the following form:

$$I_{det}(z) = A\left(\frac{\sin(k_1 z + \varphi_1)}{k_1 z + \varphi_1}\right)^2 \cos^2(k_2 z + \varphi_2) + B\left(\frac{\sin(k_1 z + \varphi_1)}{k_1 z + \varphi_1}\right)^2. \qquad (2)$$

In this case, A is the maximum amplitude of the modulated part of the function whereas B is the maximum amplitude of the unmodulated 'internal background'. As equation (2) shows, $A + B$ adds up to the maximum of $I_{det}(z)$. Thus, the modulation contrast R is equal to $B/(A + B)$. The phasefactor is given by φ_1 (enveloping curve) and φ_2 (modulation curve).

3. Results

We analysed the axial intensity distribution (AID $= I_{det}(z)$) of several objects of the same actual size to obtain an average value of the measured size. To indicate the error, the standard deviation (SD) of the single size measurements was used. We evaluated seven objects with an actual size of $d = 200$ nm, 14 objects with an actual size of $d = 140$ nm, 13 objects with an actual size of $d = 100$ nm, eight objects with an actual size of $d = 71$ nm and 11 objects with an actual size of $d = 57$ nm. The results are presented in table 1 and figure 5.

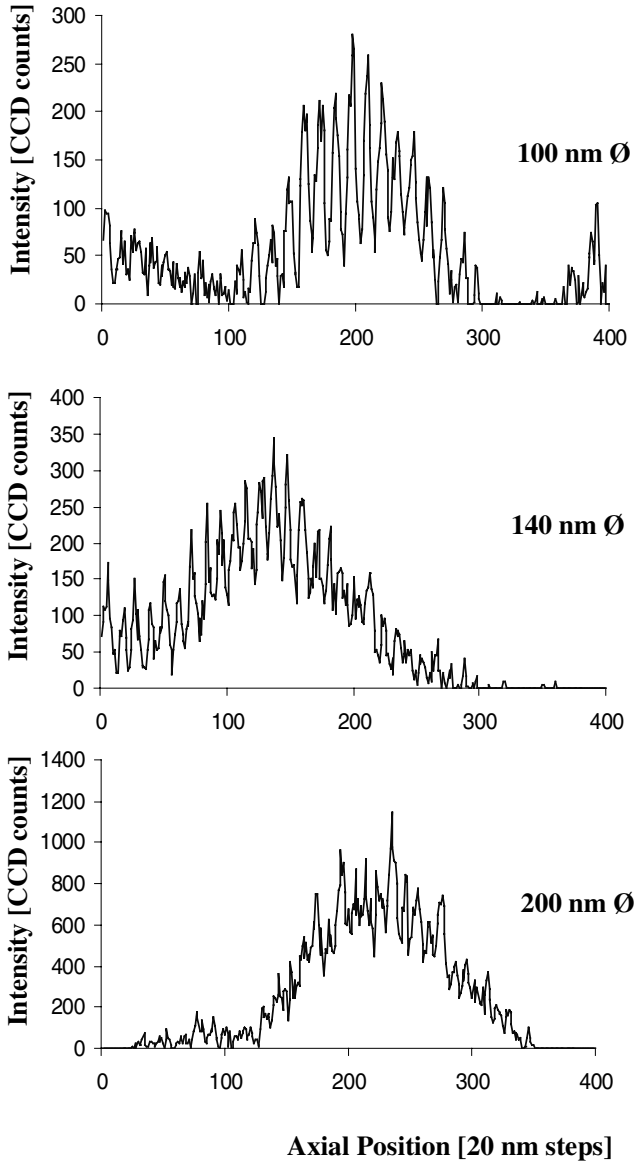

Figure 4. Experimentally achieved axial intensity distributions of green fluorescent beads with actual sizes (diameter d, given by the manufacturer) of 100, 140 and 200 nm.

These results show that the measured object sizes estimated by SMI-nanosizing at $\lambda_{ex} = 458$ nm one-photon excitation are close to the actual sizes given by the manufacturer. For the objects with an actual size of $d = 57$ nm we evaluated a size of $d = 78 \pm 8$ nm. Furthermore, we measured sizes of $d = 93 \pm 5$ nm for 71 nm objects, $d = 103 \pm 12$ nm for 100 nm objects, $d = 126 \pm 9$ nm for 140 nm objects and $d = 150 \pm 14$ nm for 200 nm objects. It can be observed that smaller objects were measured slightly larger, whereas larger objects were evaluated slightly smaller than their actual sizes. This can be explained by the fact that the measured object size depends on the form of the object and the dye distribution within the object. Here, we assume a Gaussian dye distribution. Assuming spherical dye distributions,

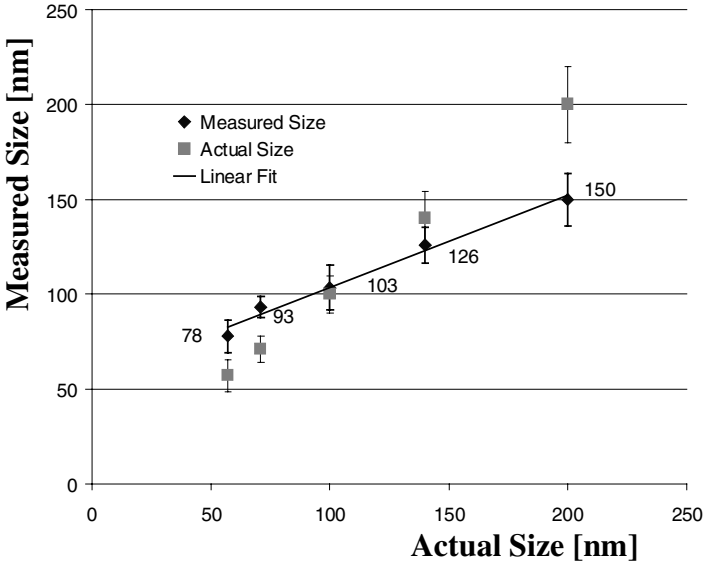

Figure 5. Mean values of SMI size measurements on green fluorescent beads as a function of the actual size (see table 1). The error is given by the standard deviation of the single measurement. The actual object sizes are given for a comparison on the abscissa.

larger object sizes will be estimated with the same modulation (see below). The error given by the manufacturer depends on the size: for the 57 nm microspheres the standard deviation given by Duke Scientific Corporation is less than 15%; for the other microspheres it is less than 10% of the mean value.

3.1. The comparison between size-measurements by SMI microscopy and a CLSM

To compare the SMI-nanosizing results to those obtained by conventional high performance fluorescence light microscopy, measurements of the AIDs of the same type of microspheres were performed using a commercial confocal laser scanning microscope (CLSM). We used the same object slides as were used during the measurements with the SMI microscope. The objects were excited by a laser beam with a wavelength of $\lambda_{ex} = 488$ nm. The full-width-at-half-maximum ($FWHM_{beads}$) of the measured signal intensity distributions in the direction of the optical axis (z) of the CLSM and in the object plane (x, y) was regarded as an appropriate measure to characterize the axial (z) and lateral (x, y) intensity distributions, respectively. Although we found that the axial $FWHM_{beads}$ appeared to have a weak linear dependence on the object size, it was not possible to determine especially axial diameters smaller than the excitation wavelength using a CLSM. In addition, the large standard deviations did not even allow us qualitatively to discriminate the smaller and the larger objects from each other.

For the lateral CLSM $FWHM_{beads}$ results, a reasonable estimate was obtained only for the 200 nm diameter beads. On the qualitative level, only 71 nm diameter beads suggested a significantly smaller size than 200 nm diameter beads. Quantitatively, for object diameters $\leqslant$140 nm, no useful size determination was achieved, in accordance with general theoretical expectations. A major problem was the low signal-to-noise ratio (SNR) when measuring the small objects. These SNRs are listed in table 2.

Because of the low SNR for the data of the smaller objects ($d = 57$ and 71 nm) it was difficult to determine an appropriate Gaussian fit function for the confocal axial intensity

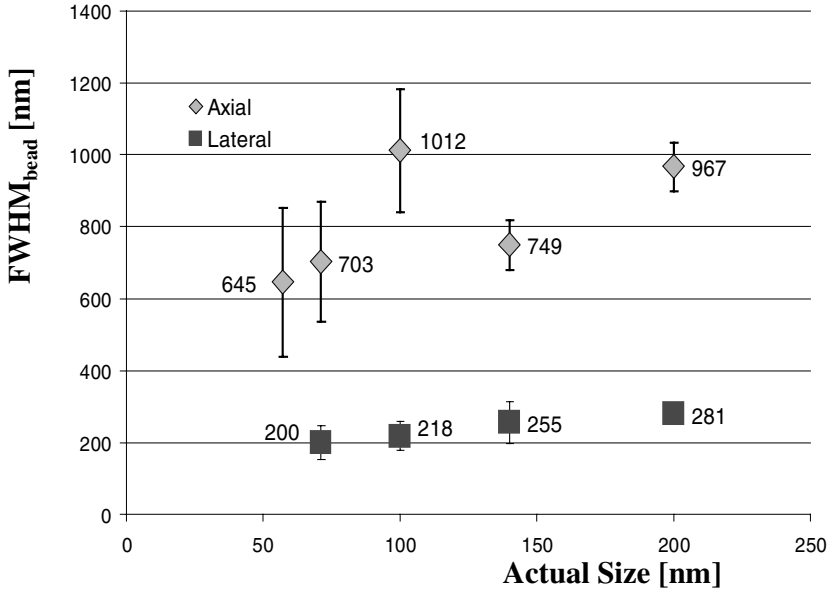

Figure 6. Measurements of the axial and lateral $FWHM_{bead}$ of green fluorescent beads using a CLSM (see table 3). Here, the mean values of $FWHM_{bead}$ are provided with an error given by the standard deviation of the single measurement.

Table 2. The signal-to-noise ratio when measuring differently sized objects using a confocal laser scanning microscope (CLSM, Leica NT).

Actual size (nm)	SNR
57	2
71	5
100	8
140	15
200	31

Table 3. FWHM of the axial and lateral intensity distribution when measuring objects from $d = 57$ to 200 nm by confocal laser scanning microscopy. There is no clear dependence of the $FWHM_{bead}$ from the object size, i.e. it is not possible to determine axial diameters of small fluorescent objects by a CLSM.

Actual size (nm)	$FWHM_{bead}$ axial (nm)	$FWHM_{bead}$ lateral (nm)	Number of objects measured
57	645 ± 210	—	10
71	703 ± 180	200 ± 48	10
100	1012 ± 180	218 ± 40	22
140	749 ± 80	255 ± 59	10
200	967 ± 80	281 ± 18	10

distributions. That is the reason why the FWHM values (table 3 and figure 6) of those objects are given with a high error and have to be understood as guide values only.

To clearly point out the different potentials of these two microscopy methods, a comparison of the colocalization volumes of the measured objects may be reasonable. Considering objects with an actual size of 100 nm, we measured a size of around 103 nm with the SMI

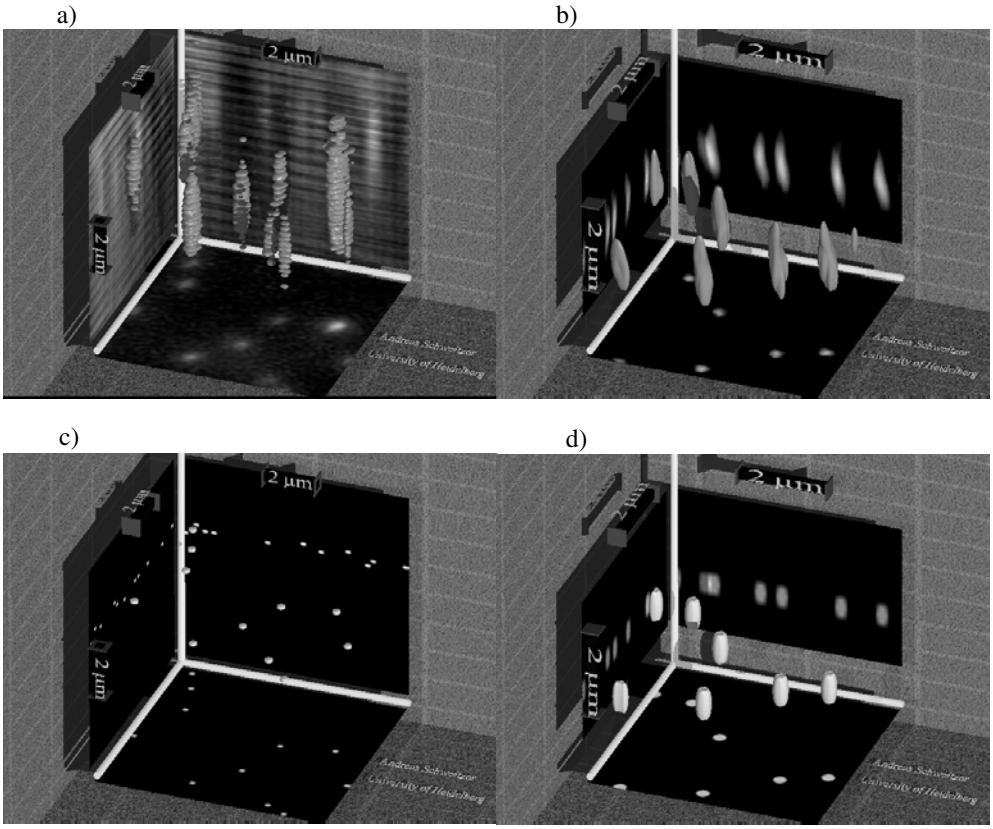

Figure 7. A 3D visualization of measured (a) SMI microscopy at $\lambda_{ex} = 458$ and (b) CLSM raw data. A visualization of spherical objects with sizes derived from the measurements is shown in (c) for SMI microscopy and in (d) for the CLSM. The size of the measured beads was $d = 140$ nm.

microscope, around 218 nm (lateral) and 1012 nm (axial) using a CLSM. Assuming spherical objects, the colocalization volumes derived from the size values are 5.2×10^{-4} μm^3 (actual), 5.7×10^{-4} μm^3 (SMI), 5.4×10^{-3} μm^3 (lateral CLSM) and 5.4×10^{-1} μm^3 (axial CLSM). Thus the colocalization volume of small objects may be estimated at least by one order of magnitude better with the SMI microscopy compared to a CLSM.

To visualize the very large difference in colocalization volumes, figures 7(a), (b) show a 3D representation of the measured raw data (bead diameter $d = 140$ nm) obtained (a) in the SMI microscope ($\lambda_{ex} = 458$ nm excitation) and (b) in the CLSM ($\lambda_{ex} = 488$ nm excitation). While the projection on the x, y plane (object plane) indicates a comparable optical lateral resolution which even appears to be somewhat better in the CLSM, the intensity distribution in the axial (z) direction is highly structured in the SMI case (figure 7(a)) but not in the CLSM case (figure 7(b)). In figures 7(c), (d), the sizes (diameters) of these spherical objects were visualized at the same scale, as calculated from the AIDs of the SMI measurements (figure 7(c)) and from the $\mathrm{FWHM}_{\mathrm{beads}}$ of the CLSM (figure 7(d)), respectively. The large difference in size determination and the far superior nanosizing by the SMI approach is obvious.

In many biological applications such as the nanosizing of large protein complexes, x-ray crystallographic results indicate that as a first approximation, a roughly spherical enveloping surface may be assumed. In this case, SMI microscopy with axial modulation only as used here

might be sufficient. For more refined studies, a lateral modulation mode might be added [22] to the axial one, making possible nanosizing not only in the axial direction (along the optical axis, z) but also in the lateral one (object plane; x, y).

4. Discussion

The data presented in this report point out that it is possible to measure sizes of fluorescent objects far below the excitation wavelength of $\lambda_{ex} = 458$ nm by using SMI microscopy. The measured values differed only slightly from the actual values. For object diameters $\leqslant 140$ nm, the deviation was $\leqslant \lambda/20$ of the exciting wavelength used. The data presented here were evaluated assuming a Gaussian dye distribution. Other distributions, for example spherical dye distributions, lead to somewhat lower R-values for the same sizes. Therefore, the modulation contrast R can vary by at least a factor of 2 which depends on the fluorochrome distribution within the object for the same object size. Other effects that cannot be neglected are small variations in the excitation field, which may be caused by varying thickness of the mounting medium between object slide and cover slip, or by stray reflections of the laser light.

Furthermore, the results confirmed that these size evaluations cannot be performed using conventional confocal laser scanning microscopy, in accordance with the theoretical expectations. Obviously, in the size range used, the $FWHM_{bead}$ of the confocal axial intensity distribution practically does not depend on the object size. From a theoretical point of view one would expect slightly lower $FWHM_{bead}$-values for smaller objects. Those changes are very difficult to detect because of experimental difficulties such as noise. The underlying reason why it is possible to measure subwavelength-sizes using SMI microscopy, but not using a CLSM, is that the SMI-AID is highly structured, and thus small changes in the object size will have an enormous effect on the AID.

In the present 458 nm SMI set-up, object diameters below 200 nm were determined substantially better than with conventional confocal microscopy. This was true not only if the confocal axial intensity distribution was used but also for the confocal lateral one. Compared with SMI-nanosizing realized at $\lambda_{ex} = 488$ and 647 nm (see [20, 25]), however, the nanosizing capability below 100 nm diameter so far turned out to be less satisfying. A main reason for this may be seen for example in the relatively high noise level encountered here. This may be because of a variety of reasons due to the object and to the presently realized detection mode. We anticipate that such problems may be overcome in the near future. Consequently, in the long term we expect that by using this smaller wavelength of $\lambda_{ex} = 458$ nm in comparison to the recently presented size measurements using $\lambda_{ex} = 488$ and 647 nm [20], it should be possible to extend nanosizing to even somewhat smaller object sizes.

The combination of different excitation wavelengths for SMI-nanosizing opens highly interesting novel perspectives in the light optical nanoscopy of biomolecular machines [23]. Here, we want to restrict ourselves to a special example, gene expression SMI microscopy [23]: the basic idea is to use the difference in condensation of actively transcribed genes versus non-transcribed genes. This would allow us to estimate the transcription potential of specific genes in individual cells by (a) specifically labelling a gene, and (b) measuring the size of the identified gene region by SMI-nanosizing. Most interestingly, a combinatorial labelling of the genes should be possible. Assuming a spectral signature 1 excited by $\lambda_{ex} = 458$ nm, a spectral signature 2 excited by $\lambda_{ex} = 488$ nm; and a spectral signature 3 excited by $\lambda_{ex} = 647$ nm, by combinatorial labelling up to 7 objects optically isolated from each other (i.e. distance larger then the optical resolution) could be identified and 'nanosized'. An extension to more spectral signatures, e.g. $N = 7$, would allow the combinatorial identification of $n = 2^N - 1 = 127$ different genes in a given cell nucleus. The maximum number of genes to be identified in a nucleus would be given by the optical resolution of the SMI system and in principle amount

to several thousands of genes. One straightforward possibility to realize 'Multiplex' SMI microscopy with a variety of exciting wavelengths would be to use an addressable cell localization system and to perform the SMI measurements subsequently. For example, one might register the 488 and 647 nm fluorescence in a 488/647 SMI set-up, then transfer the specimen to the 458 nm SMI microscope, and register the same cells again. A more advanced SMI instrument would combine the different excitation and fluorescence detection modes in one instrument.

Eventually, such a 'multiplex gene expression microscopy' based on the SMI-nanosizing approach might contribute to the high throughput testing of gene activity modifying pharmaceutical agents on the cell-by-cell level. A rough estimate suggests that in this way, per year and multiplex-SMI device, up to thousands of substances might be tested for their specific transcription modifying potential. It is obvious that such long term developments would require substantial further developments in multicolour molecular labelling, SMI technology, and automated image analysis.

Acknowledgments

This work was supported by the Bundesminister für Bildung und Forschung (BMBF) and the Deutsche Forschungsgemeinschaft (DFG). We thank Dr Benno Albrecht, Dr Antonio Virgilio Failla, Dr Christian Carl and Dr Udo Spöri for stimulating discussions.

References

[1] O'Brien T B, Bult C J, Cremer C, Grunze M, Knowles B B, Langowski J, McNally J, Pederson T, Politz J C, Pombo A, Schmahl G, Spatz J P and van Driel R 2003 *Genome Res.* **13** 1–13
[2] Lamond A I and Earnshaw W C 1998 *Science* **280** 547–53
[3] Cremer T and Cremer C 2001 *Nat. Rev. Genet.* **2** 292–301
[4] Hell S W, Lindek S and Stelzer E H K 1994 *J. Mod. Opt.* **41** 675–81
[5] Hell S W, Stelzer E H K, Lindek S and Cremer C 1994 *Opt. Lett.* **19** 222–4
[6] Hell S W, Lindek S, Cremer C and Stelzer E H K 1994 *Appl. Phys. Lett.* **64** 1335–7
[7] Klar T A, Jacobs S, Dyba M, Egner A and Hell S W 2000 *Proc. Natl Acad. Sci. USA* **87** 8206–10
[8] Dyba M and Hell S W 2002 *Phys. Rev. Lett.* **88** 163901
[9] Dyba M and Hell S W 2003 *Appl. Opt.* **42** 5123–9
[10] Bailey B, Farkas D L, Taylor D L and Lanni F 1993 *Nature* **366** 44–8
[11] Schneider B, Bradl J, Kirsten I, Hausmann M and Cremer C 1998 *Fluorescence Microscopy & Fluorescence Probes* vol 2, ed J Slavik (New York: Plenum) pp 63–8
[12] Failla A V and Cremer C 2001 *Optical Diagnostics of Living Cells IV* ed D L Farkas and R C Leif; *Proc. SPIE* **4260** 120–6
[13] Albrecht B, Failla A V, Schweitzer A and Cremer C 2002 *Appl. Opt.* **41** 80–7
[14] Gustafsson M G, Agard D A and Sedat J W 1995 *Three-Dimensional Microscopy: Image Acquisition and Processing II* ed T Wilson and C J Cogswell; *Proc. SPIE* **2412** 147–56
[15] Heintzmann R, Jovin Th M and Cremer Ch 2002 *J. Opt. Soc. Am.* A **19** 1599–609
[16] Gustafsson M G 2002 *J. Microsc.* **198** 82–7
[17] Lindek S, Stelzer E H K and Hell S W 1995 *Handbook of Biological Confocal Microscopy* ed J B Pawley (New York: Plenum) pp 417–30
[18] Bornfleth H, Sätzler K, Eils R and Cremer C 1998 *J. Microsc.* **189** 118–36
[19] Failla A V, Cavallo A and Cremer C 2002 *Appl. Opt.* **41** 6651–9
[20] Failla A V, Spoeri U, Albrecht B, Kroll A and Cremer C 2002 *Appl. Opt.* **41** 7275–83
[21] Albrecht B, Failla A V, Heintzmann R and Cremer C 2001 *J. Biomed. Opt.* **6** 292–9
[22] Frohn J T, Knapp H F and Stemmer A 2002 *Opt. Lett.* **26** 828–30
[23] Failla A V, Albrecht B, Spöri U, Schweitzer A, Kroll A, Hildenbrand G, Bach M and Cremer C 2003 *ComPlexUs* **1** 77–88
[24] Wagner C *et al* 2004 Unpublished results
[25] Spoeri U *et al* 2004 *J. Appl. Phys.* at press